1

The following publication Z. Xu, Y. Xiao and W. Chen, "Robust Correspondence Imaging Against Random Disturbances With Single-Pixel Detection," in IEEE Transactions on Computational Imaging, vol. 11, pp. 901-910, 2025 is available at https://doi.org/10.1109/TCI.2025.3577334.

Robust Correspondence Imaging against Random Disturbances with Single-Pixel Detection

Zhihan Xu, Yin Xiao, and Wen Chen

Abstract—Random disturbance has become a great challenge for correspondence imaging (CI) due to dynamic and nonlinear scaling factors. In this paper, we propose a robust CI against random disturbances for high-quality object reconstruction. To remove the effect of dynamic scaling factors induced by random disturbance, a wavelet and total variation (WATV) algorithm is developed to estimate a series of varying thresholds. Then, light intensities collected by a single-pixel detector are processed by using the series of estimated varying thresholds. To realize highquality object reconstruction, the binarized light intensities and a series of random patterns are fed into a plug-and-play priors (PnP) algorithm with an iteration framework and a general denoiser, called as CI-PnP. Theoretical descriptions are given in detail to reveal the formation mechanism in CI under random disturbance. Optical measurements are conducted to verify robustness of the proposed CI against random disturbances. It is demonstrated that the proposed method can remove the effect of dynamic scaling factors induced by random disturbance, and can realize high-quality object reconstruction. The proposed method provides a promising solution to achieving ultra-high robustness against random disturbances in CI, and is promising in various applications.

Index Terms—Correspondence imaging, High-quality object reconstruction, Random disturbance, Complex environments, Single-pixel detection.

I. INTRODUCTION

MAGING systems usually received information-carrying light fields by utilizing a pixelated sensor such as charge-coupled device (CCD) or complementary metal-oxide-semiconductor (CMOS) [1], [2], which can capture 2D images related to the intensity distributions of light field. To accurately extract useful information from the captured images, disturbance induced by the environment or imaging system needs to be avoided. However, random disturbance could be inevitable in practice [3], such as thermal noise in electronic devices [4], ambient light [5]–[8] and turbulence in an optical channel [9]–[12], leading to noisy measurement and inaccurate information extraction. Therefore, imaging against

This work was supported by the Hong Kong Research Grants Council (15224921, 15223522) and The Hong Kong Polytechnic University (1-WZ4M, 1-CDJA). (Corresponding author: Wen Chen)

Zhihan Xu is with the Department of Electrical and Electronic Engineering, The Hong Kong Polytechnic University, Hong Kong, China (e-mail: zhihan.xu@connect.polyu.hk).

Yin Xiao is with the Department of Electrical and Electronic Engineering, The Hong Kong Polytechnic University, Hong Kong, China (e-mail: yinxiao@polyu.edu.hk).

Wen Chen is with the Department of Electrical and Electronic Engineering & Photonics Research Institute, The Hong Kong Polytechnic University, Hong Kong, China (e-mail: owen.chen@polyu.edu.hk).

random disturbance has attracted much attention, especially when imaging systems are deployed in complex or extreme environments where random disturbance overwhelms, such as satellite imagery [13]–[15], underwater imaging [16]–[18] and capsule endoscopy [19], [20] etc. Random disturbance induced in such environments introduces difficulties for the existing imaging systems, and becomes a challenge to visualizing an object or extracting clear information.

To overcome the challenges induced by random disturbance, ghost imaging (GI) emerged as a promising solution [21]-[23]. By projecting a series of illumination patterns onto an unknown object and measuring light using a single-pixel detector, computationally realize object reconstruction [24]-[30]. The advantages of GI lie in several aspects. For instance, singlepixel detectors could precisely provide temporal resolution, making it feasible in 3D imaging [31], [32] and ultrafast imaging [33]. Compared to the pixelated detectors, singlepixel detectors show the higher efficiency and sensitivity in a wide spectrum (e.g., infrared [34], [35], terahertz [36], [37] and X-ray [38], [39]). More importantly, GI encodes 2D spatial information into a 1D signal to be processed in a flexible manner. Moreover, it can provide advantages over 2D imaging, when the disturbance exists. In recent years, correspondence imaging (CI) has been developed as an alternative [40]-[43], when a single-pixel detector is used. Without the usage of single-pixel light intensities as correlation coefficients, CI adopts a binarization of collected light intensities with a constant threshold to divide the series of illumination patterns into two groups. By superimposing the classified illumination patterns in each group, two reconstructed patterns can be obtained with positive and negative contrasts respectively called as positive and negative images. A higher-quality reconstructed object image can be generated by subtracting the negative image from the positive image [40], [41]. With the binarized light intensities, CI could offer the higher efficiency in data storage, data transmission and object reconstruction. Compared to GI, CI could also be insensitive to nonlinear distortions occurring in noisy environments [44].

Although CI was demonstrated to be promising for object reconstruction, its feasibility under random disturbance is still limited. Most existing studies focus on the applications of CI in free space without disturbance. Although CI was studied [44]–[48], few studies focus on CI against random disturbance from multiple sources which may lead to a high-level fluctuation in the collected single-pixel light intensities. The reconstruction with pattern superimposition in CI also suffers

from low quality owing to a series of random patterns used for the illumination [49], [50], posing a challenge for the potential applications. Therefore, it is significant and desirable to achieve the robustness of CI against random disturbance.

In this paper, we propose a robust CI against random disturbances. To remove the effect of dynamic and nonlinear scaling factors induced by random disturbance, a series of varying thresholds are first estimated by using a wavelet and total variation (WATV) algorithm. After single-pixel light intensities are binarized by the series of estimated varying thresholds, a plug-and-play (PnP) prior algorithm is developed and applied via designing an iteration framework and the block-matching and 3D filtering (BM3D), called as CI-PnP. A series of optical experiments are conducted to illustrate feasibility and effectiveness of the proposed method. It is demonstrated that the estimated varying thresholds can facilitate an accurate removal of the effect of dynamic scaling factors induced by random disturbance, and high-quality object reconstruction is realized.

The main contributions of our work are briefly summarized as follows:

- 1) The robustness of CI is fully studied using the varying thresholds, and ultra-high robustness against random disturbances is achieved in complex environments.
- 2) A regularized computational algorithm in a PnP manner is designed instead of linear correlations in conventional methods, leading to the realization of high-fidelity object reconstruction.
- 3) A detailed theoretical derivation of formation mechanism of computational CI through complex scattering media with random disturbances is presented. A series of experimental results, i.e., under various random disturbances with different parameters, are obtained to illustrate that the proposed method outperforms conventional approaches in terms of performance and efficiency.

The rest of the paper is organized as follows: The formation mechanism of CI with random disturbances in complex environments and the proposed principles are described in detail in Section II. The optical setup, experimental settings and experimental results are presented and discussed in Section III. Finally, conclusions are drawn in Section IV.

II. PROBLEM FORMULATION AND METHODS

A. Problem Formulation

In CI without disturbance, a series of random patterns are sequentially projected onto an unknown object O with the light intensities collected by a single-pixel detector [51].

$$\mathbf{s} = \mathbf{A}\mathbf{x},\tag{1}$$

where $\mathbf{A} \in \square^{M \times N}$ denotes a modulation matrix with M vectorized patterns and N pixels in each pattern, $\mathbf{x} \in \square^{N \times 1}$ denotes the unknown object vectorized as a column vector, and $\mathbf{s} = [s_1 \quad s_2 \quad \cdots \quad s_M]^T \in \square^{M \times 1}$ denotes a vector with M light intensities. It is given in Eq. (1) that there is a linear sampling

process with a sampling ratio defined by M/N, and the problem related to the sampling ratio also needs to be solved.

It was demonstrated that single-pixel light intensities collected without disturbance in free space obey a multivariate Gaussian distribution [49], when the random patterns are independent and identically distributed.

$$\mathbf{s} \sim \mathsf{N} \left(\mathbf{\mu}, \mathbf{\Sigma} \right),$$
 (2)

where $\mu \in \Box^{M \times 1}$ and $\Sigma \in \Box^{M \times M}$ denote a vector with mean values and a covariance matrix of the multivariate Gaussian distribution, respectively. The single-pixel light intensities in \mathbf{s} are independent and identically distributed, indicating that the collected light intensities share one mean value and the covariance between any two intensities is zero. Therefore, μ and Σ can be respectively described by

$$\mathbf{\mu} = \mu \mathbf{1},\tag{3}$$

$$\Sigma = \operatorname{diag}(\sigma^2 \mathbf{1}), \tag{4}$$

where $\mathbf{1} \in \square^{M \times 1}$ denotes a vector only with one, diag(·) denotes an operator to generate a diagonal matrix with its input as diagonal elements, and μ and σ denote the parameters to be approximated by using an average value and standard deviation of the single-pixel light intensities, respectively.

To retrieve object information from the series of collected single-pixel light intensities, a constant threshold is usually calculated and applied in CI to binarize the light intensities.

$$\mathbf{s}^{(\pm)} = \operatorname{Sign}(\mathbf{s} - \boldsymbol{\mu}), \tag{5}$$

where $\operatorname{Sign}(\cdot)$ denotes an operator to return ± 1 depending on the sign of its input and $\mathbf{s}^{(\pm)} \in \Box^{M \times 1}$ denotes the binarized light intensities with values of +1 and -1. A correspondence image $\tilde{\mathbf{x}}$ can be recovered by averaging random patterns conditionally depending on the signs of the binarized single-pixel light intensities.

$$\tilde{\mathbf{x}} = \frac{1}{M} \mathbf{A}^{\mathrm{T}} \mathbf{s}^{(\pm)}.$$
 (6)

When random disturbance exists in CI, the series of collected single-pixel light intensities would fluctuate significantly owing to dynamic and nonlinear scaling factors induced by random disturbance.

$$\tilde{\mathbf{s}} = \mathbf{K}\mathbf{s},$$
 (7)

where $\tilde{\mathbf{s}} = [\tilde{s}_1 \quad \tilde{s}_2 \quad \cdots \quad \tilde{s}_M]^{\mathrm{T}} \in \square^{M \times 1}$ denotes a series of single-pixel light intensities collected under random disturbance, and $\mathbf{K} = \mathrm{diag}(\mathbf{k}) \in \square^{M \times M}$ denotes a diagonal matrix generated from a vector consisting of scaling factors $\mathbf{k} = [k_1 \quad k_2 \quad \cdots \quad k_M]^{\mathrm{T}} \in \square^{M \times 1}$. Random disturbance from multiple sources could be inevitable in complex environments,

and a series of dynamic scaling factors could be induced accordingly to significantly affect the collected single-pixel light intensities.

According to a linear transform theorem for multivariate Gaussian distributions, the light intensities collected under random disturbances in complex environments obey a different multivariate Gaussian distribution compared to that in free space without disturbances.

$$\tilde{s} \sim N\left(\tilde{\mu}, \tilde{\Sigma}\right),$$
 (8)

where $\tilde{\mu}$ and $\tilde{\Sigma}$ denote a vector and a covariance matrix respectively calculated by

$$\tilde{\mathbf{\mu}} = \mathbf{K}\mathbf{\mu},\tag{9}$$

$$\tilde{\mathbf{\Sigma}} = \mathbf{K} \mathbf{\Sigma} \mathbf{K}^{\mathrm{T}}.$$
 (10)

It can be seen in Eq. (9) that vector $\tilde{\boldsymbol{\mu}}$ is disturbed by dynamic and nonlinear scaling factors. The covariance matrix $\tilde{\boldsymbol{\Sigma}}$ is still a diagonal matrix, indicating that light intensities collected under random disturbance are independent. Since $\boldsymbol{\mu}$ is a constant vector irrelevant with dynamic scaling factors, vector $\tilde{\boldsymbol{\mu}}$ is equivalent to dynamic scaling factors \boldsymbol{k} with a constant $\boldsymbol{\mu}$ described by

$$\tilde{\mathbf{\mu}} = \mathbf{K}\mathbf{\mu} = \mu \mathbf{k}.\tag{11}$$

Due to random disturbance, unknown dynamic scaling factors \mathbf{k} are randomly distributed in magnitude, and the usage of one constant threshold in Eq. (5) cannot be effective. It is demonstrated in Eq. (11) that vector $\tilde{\boldsymbol{\mu}}$ can provide information related to the series of dynamic scaling factors \mathbf{k} . Therefore, to remove the effect of dynamic scaling factors induced by random disturbance, it is feasible to estimate $\tilde{\boldsymbol{\mu}}$ as a series of varying thresholds.

B. The Varying-threshold Estimation using WATV

It can be seen in Eq. (8) that single-pixel light intensities collected under random disturbance obey a multivariate Gaussian distribution, and can be reformulated as vector $\tilde{\mu}$ added by a zero-mean Gaussian distribution.

$$\tilde{\mathbf{s}} \sim \mathsf{N}\left(\tilde{\boldsymbol{\mu}}, \tilde{\boldsymbol{\Sigma}}\right) = \tilde{\boldsymbol{\mu}} + \mathsf{N}\left(0, \tilde{\boldsymbol{\Sigma}}\right).$$
 (12)

The zero-mean Gaussian distribution has a diagonal covariance matrix $\tilde{\Sigma}$, which can be treated as Gaussian white noise. To estimate vector $\tilde{\mu}$ as varying thresholds, a WATV algorithm [52] is proposed and performed on the recorded light intensities via solving an optimization model described by

$$\hat{\mathbf{w}} = \arg\min_{\mathbf{w}} \left\{ \frac{1}{2} \|\mathbf{W}\tilde{\mathbf{s}} - \mathbf{w}\|_{2}^{2} + \lambda^{T} \mathbf{\Phi}(\mathbf{w}) + \beta \|\mathbf{D}\mathbf{W}^{T}\mathbf{w}\|_{1} \right\},$$
(13)

where W denotes a discrete wavelet transform matrix, w denotes wavelet coefficients, λ represents a regularization parameter, $\Phi(w)$ represents a penalty function utilized to promote sparsity and convexity of the objective function, and D denotes a first-order difference matrix. By solving this objective function, optimal wavelet coefficients \hat{w} can be obtained to further approximate vector $\tilde{\mu}$ by using inverse wavelet transform.

$$\tilde{\boldsymbol{\mu}} \approx \hat{\boldsymbol{\mu}} = \mathbf{W}^{\mathrm{T}} \hat{\mathbf{w}}. \tag{14}$$

Then, vector $\hat{\boldsymbol{\mu}} = [\hat{\mu}_1 \quad \hat{\mu}_2 \quad \cdots \quad \hat{\mu}_M]^T$ is employed as a series of varying thresholds for a binarization of the series of single-pixel light intensities collected under random disturbance. A binarizer using the estimated varying thresholds can be described by

$$\tilde{\mathbf{s}}^{(\pm)} = \operatorname{Sign}(\tilde{\mathbf{s}} - \hat{\boldsymbol{\mu}}) \approx \operatorname{Sign}(\tilde{\mathbf{s}} - \tilde{\boldsymbol{\mu}})$$

$$= \operatorname{Sign}(\mathbf{K}\mathbf{s} - \mathbf{K}\boldsymbol{\mu})$$

$$= \operatorname{Sign}(\mathbf{K}(\mathbf{s} - \boldsymbol{\mu})) \qquad . \tag{15}$$

$$= \operatorname{Sign}(\mathbf{s} - \boldsymbol{\mu})$$

$$= \mathbf{s}^{(\pm)}$$

It can be seen in Eq. (15) that using the proposed algorithm, the binarized light intensities obtained by using the series of estimated varying thresholds in CI under random disturbance approximate to those obtained by using a constant threshold in CI without any disturbances.

C. The CI-PnP

After the series of single-pixel light intensities is binarized by using the estimated varying thresholds in Eq. (15), object information can be further retrieved by using the binarized light intensities and the series of random patterns. A correspondence image recovered based on conventional CI in Eq. (6) suffers from low quality, since it only considers conditional averaging among the series of random patterns. Here, with the binarization in Eq. (15), the nonlinearly inverse problem cannot be completely solved by a linear operation in Eq. (6). A CI-PnP method is further developed and applied by designing an optimization model described by

$$\hat{\mathbf{x}} = \arg\min_{\mathbf{x}} \left\{ \mathsf{D}(\mathbf{x}) + \mathsf{R}(\mathbf{x}) \right\},\tag{16}$$

where D(x) denotes a data-fidelity term to ensure that a reconstructed object \hat{x} is consistent with the measured data (i.e., the light intensities binarized by the estimated varying thresholds) defined by

$$D(\mathbf{x}) = -\frac{1}{M} \left\langle \mathbf{A} \mathbf{x}, \tilde{\mathbf{s}}^{(\pm)} \right\rangle, \tag{17}$$

and R(x) denotes a regularization term to preserve the pre-

defined properties, i.e., sparsity in spatial domain and a *prior* $R_{BM3D}(\mathbf{x})$ implicitly defined by BM3D [53], [54], described by

$$\mathsf{R}(\mathbf{x}) = a \|\mathbf{x}\|_{1} + b \mathsf{R}_{BM3D}(\mathbf{x}), \tag{18}$$

where $\|\cdot\|_1$ denotes the L1 norm, and a and b denote regularization parameters. To solve the optimization model in Eq. (16), a PnP priors approach is utilized by introducing an iteration framework and BM3D [53], [54], and the details are given in **Algorithm 1**. In **Algorithm 1**, L denotes the total iteration number. A gradient descent step is introduced with a step size γ in Line 2 of **Algorithm 1** to minimize the data-fidelity term $D(\mathbf{x})$. To reduce the first component in Eq. (18), a proximal operator is used in Line 3 of **Algorithm 1** defined by

$$Soft_{a_l}(\mathbf{x}) = Sign(\mathbf{x}) \cdot max(|\mathbf{x}| - a_l, 0). \tag{19}$$

In Line 4 of **Algorithm 1**, a BM3D denoiser $f_{b_i}(\cdot)$ is chosen to suppress the artefacts of the estimated reconstruction during the iterations. To avoid over-filtering, a data fusion step is designed to combine the estimations in two successive iterations with different weights, as shown in Line 5 of **Algorithm 1**. In addition, parameters are fine-tuned for the next iteration in Lines 6–8 of **Algorithm 1**. After all the iterations are completed, a high-quality reconstructed object image can be rendered. It is worth noting that **Algorithm 1** can be considered as a proximal-gradient version of PnP because of the usage of a proximal operator in Eq. (19) and the alternating minimization manner.

Algorithm 1: CI-PnP

Input: A, $\tilde{\mathbf{s}}^{(\pm)}$, η , γ , $\mathbf{q}^{-1} = \mathbf{0}$ **Initiating** $a_0, b_0, \theta_0, \mathbf{x}^0$

- 1. for $l \leftarrow 0$ to L-1 do
- 2. $\mathbf{x}^{\prime l} \leftarrow \mathbf{x}^{l} \gamma \nabla \mathsf{D}(\mathbf{x}^{l})$
- 3. $\mathbf{z}^l \leftarrow \operatorname{Soft}_a(\mathbf{x}^{\prime l})$
- **4.** $\mathbf{q}^l \leftarrow f_b(\mathbf{z}^l)$
- 5. $\mathbf{x}^{l+1} \leftarrow (1-\theta_l)\mathbf{q}^l + \theta_l\mathbf{q}^{l-1}$
- **6.** $\theta_{l+1} \leftarrow \eta \theta_l$
- 7. $a_{i+1} \leftarrow \eta a_i$
- **8.** $b_{l+1} \leftarrow \eta b_l$
- 9. end

Output: $\hat{\mathbf{x}} = \mathbf{x}^L$

D. Algorithm Description

The proposed robust CI against random disturbances is

further shown in Fig. 1. A series of random patterns are sequentially projected onto an unknown object with optical waves propagating in free space under random disturbance induced from multiple sources. The light field is measured by using a single-pixel detector. A binarizer is designed and applied to process the light intensities, and then the results are fed into the CI-PnP to reconstruct an unknown object. Here, as a typical example, random disturbance is generated simultaneously from three sources, i.e., random disturbance in light source, random disturbance in complex media, and random disturbance in the detector.

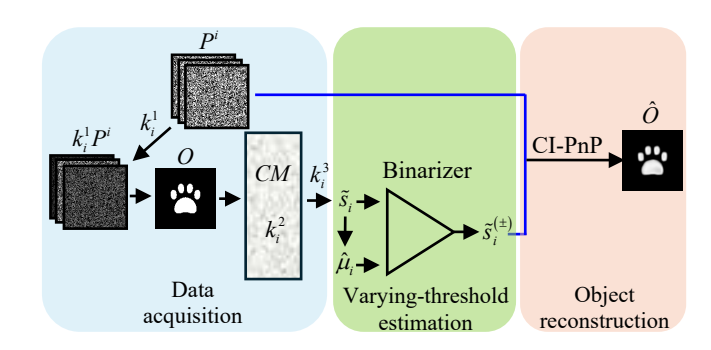


Fig. 1. A schematic for the proposed robust CI under random disturbances. P^i : the ith illumination pattern; k_i^1 , k_i^2 and k_i^3 : dynamic scaling factors induced by random disturbance respectively generated in light source, complex media and the single-pixel detector; CM: complex media; \bar{s}_i : single-pixel light intensities recorded under random disturbance; $\hat{\mu}_i$: the estimated varying threshold; $\bar{s}_i^{(\pm)}$: the binarized light intensities obtained by using a series of estimated varying thresholds; \hat{o} : a reconstructed object image.

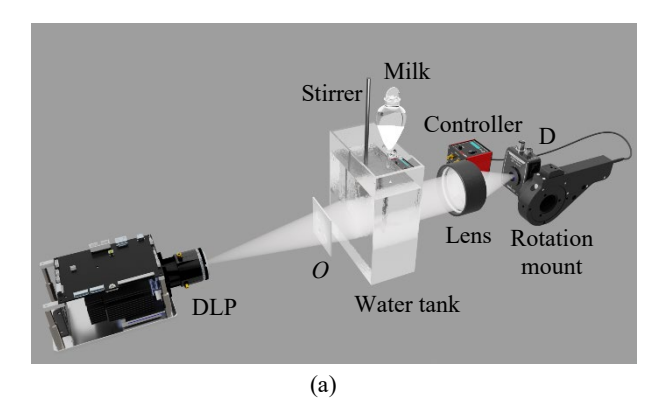
III. EXPERIMENTAL RESULTS AND DISCUSSION

A. An Optical Setup

A series of optical experiments are conducted to show the proposed robust CI against random disturbances in complex environments. The experimental setup is shown in Figs. 2(a) and 2(b).

A digital light projector (Texas Instrument, DLP4710EVM-LC) is used, consisting of a 1920×1080 digital micromirror device (DMD) and three light-emitting-diode (LED) channels. The LED currents in three channels can be controlled arbitrarily within a preset range, and brightness of the projector can be arbitrarily adjusted in order to illustrate random disturbance in light source. The larger adjustment range of LED currents could represent a higher disturbance level. All LED channels are switched on to sequentially generate a series of random patterns (binary values of 0 and 1) with 128×128 pixels during the measurements. The illumination patterns are sampled to ensure that they are independent and identically distributed. An unknown object is placed in focus to be illuminated by random patterns. To illustrate random disturbance generated in complex media, optical waves propagate in a dynamic and turbid water environment created by using a transparent polymethyl

methacrylate-made water tank with 10.0 cm (length) $\times 20.0 \text{ cm}$ (width) $\times 30.0 \text{ cm}$ (height) where 3000.0-ml pure water is placed. During the measurements, a pear-shaped funnel is used to continuously drop milk solutions composed of 200-ml clean water and 40-ml milk into water tank, and a stirrer keeps rotating with a speed of 500.0 rpm. After wave propagation through complex media, the scrambled light field is collected



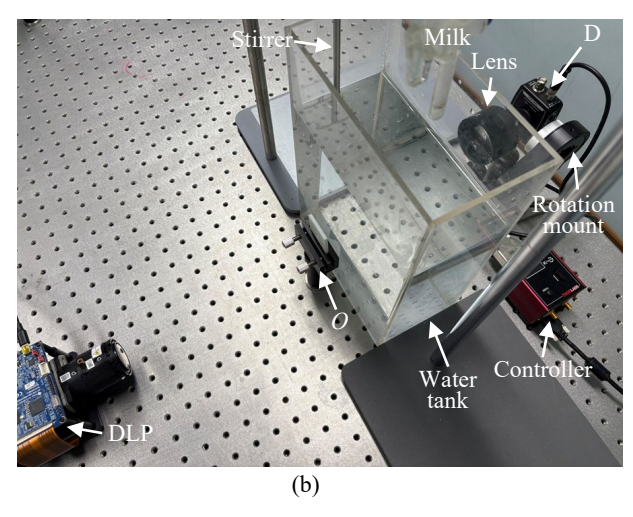


Fig. 2. (a) A schematic experimental setup for the proposed robust CI against random disturbance in complex environments, and (b) a photo of the actual setup. DLP: digital light projector; D: single-pixel bucket detector; O: object.

by a lens with a focal length of 10.0 cm and then received by a single-pixel detector (Thorlabs, PDA100A2). The detector has switchable light responses different among automatically controlled by a motorized precision rotation mount (Thorlabs, PRM1Z8) and a DC servo motor controller (Thorlabs, KDC101) to show random disturbance at the receiver. More gain settings and a larger range of the switching frequencies could represent a higher disturbance level at the receiver. Random disturbance generated in the detector by arbitrarily switching the gains is more severe compared to others, such as background noise in the detection and temperature drift. Finally, the single-pixel light intensities are sequentially collected by recording the photocurrents with the single-pixel detector via a data-acquisition device (ART Technology, USB8586). All optical experiments reported here

are conducted under white light illumination rather than in a dark room to illustrate robustness of the proposed CI system against ambient light, and random disturbance is generated simultaneously from multiple sources.

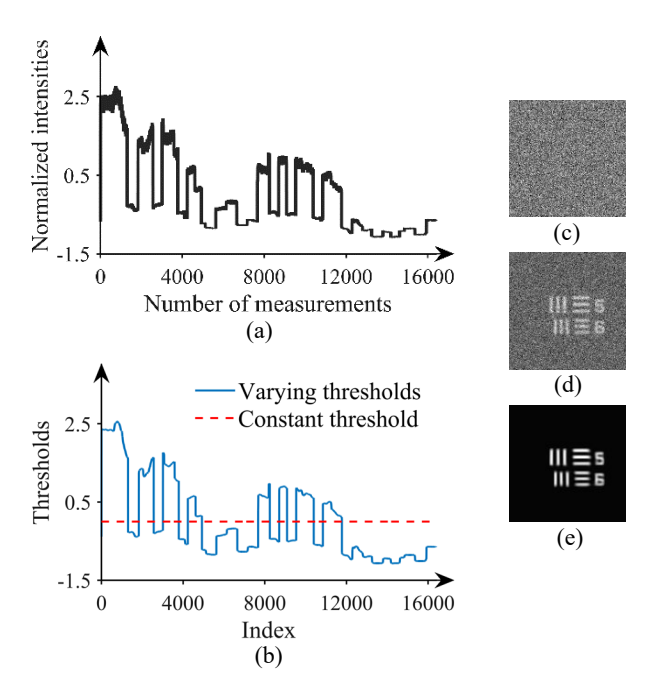


Fig. 3. Experimental results in the CI under random disturbance to test USAF 1951 resolution target (elements 5 and 6 of group -1): (a) the normalized single-pixel light intensities, (b) a constant threshold via calculating an average value of the normalized light intensities and the varying thresholds estimated by using the proposed WATV algorithm, (c) a correspondence image recovered by using CI with a constant threshold, (d) a correspondence image obtained by using CI with the estimated varying thresholds, and (e) a reconstructed object obtained by using the proposed CI-PnP with the estimated varying thresholds. The normalization operation is conducted by subtracting an average value of collected light intensities and divided by standard deviation. Here, random disturbance is generated simultaneously from three sources, i.e., random disturbance in light source, random disturbance in complex media, and random disturbance in the detector.

B. A Resolution Target

Spatial resolution is defined as the ability of an imaging system to resolve details of an object to be imaged, as a crucial parameter to evaluate the imaging performance and associated algorithms. A USAF 1951 resolution target is first tested in optical experiments, consisting of several groups of line elements with defined thicknesses and spacing. By identifying the finest line elements in the recovered USAF 1951 resolution target, achievable resolution can be determined for the designed experimental setup. The light field is collected by a single-pixel detector under random disturbance as shown in Fig. 3(a), and then is fed into the proposed algorithm for object reconstruction. Element 6 of group -1 is well resolved with a linewidth of 561.23 µm as shown in Fig. 3(e), and the number of realizations is 16384. In this experiment, LED currents of the projector are controlled in a range of 200 mA-

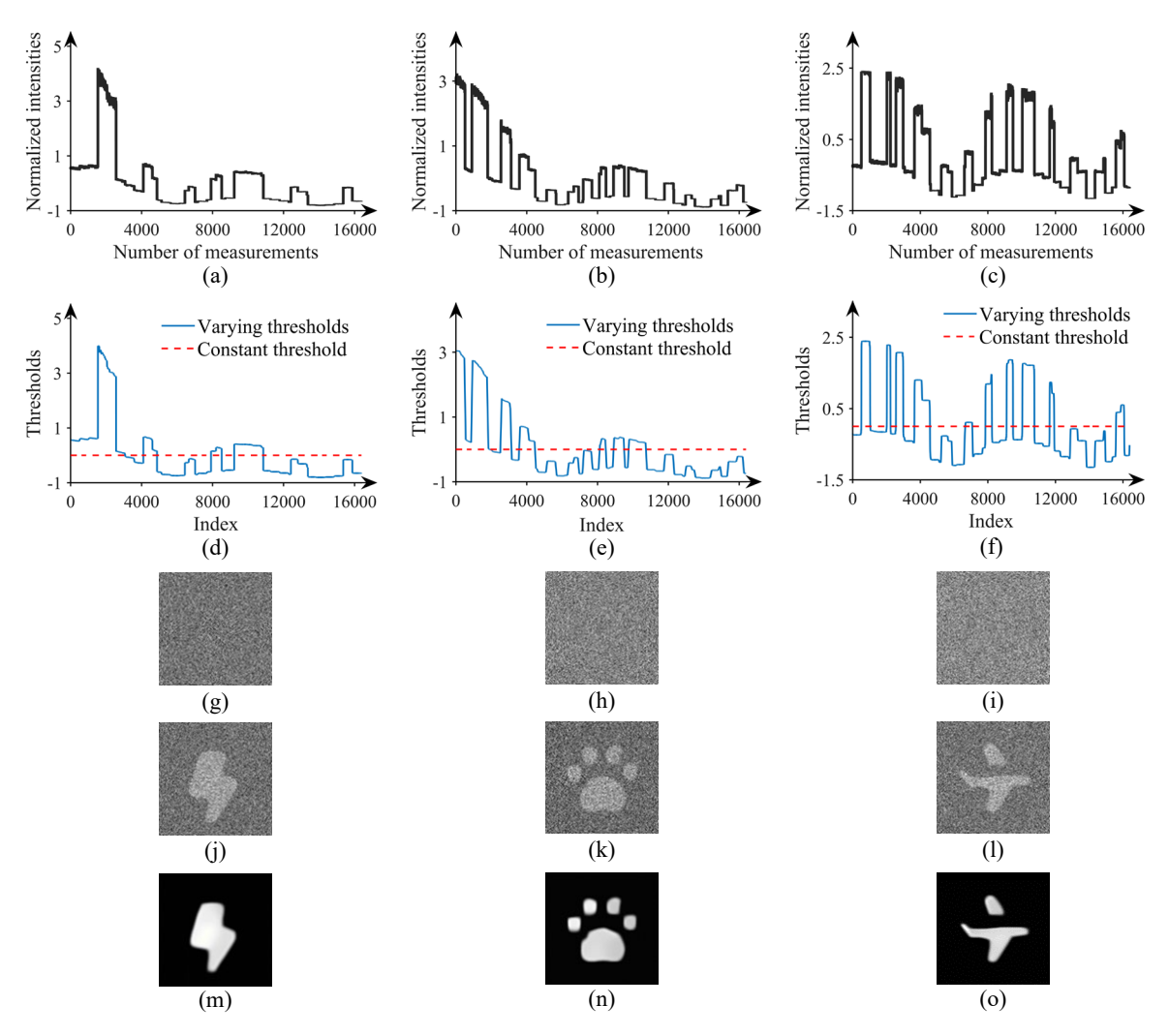


Fig. 4. Experimental results corresponding to the objects 1-3 in CI under random disturbances with different disturbance levels: (a)-(c) the normalized single-pixel light intensities, (d)-(f) constant thresholds obtained by calculating an average value of the light intensities and the varying thresholds estimated by using the developed WATV algorithm, (g)-(i) correspondence images obtained by using CI with a constant threshold, (j)-(l) correspondence images obtained by using CI with the estimated varying thresholds, and (m)-(o) the reconstructed object images obtained by using the proposed CI-PnP with the estimated varying thresholds. The random disturbance is created simultaneously from three sources, i.e., random disturbance in light source, random disturbance in complex media, and random disturbance in the detector.

500 mA, and light responses of the detector are switched with two gains of 0 dB and 10 dB. Gain switching frequencies are arbitrarily chosen in a range of 0.5 min⁻¹ to 1.0 min⁻¹.

Figure 3(a) shows the collected single-pixel light intensities at the receiver. It can be seen in Fig. 3(a) that the collected light intensities fluctuate significantly with multiple abrupt changes owing to dynamic and nonlinear scaling factors induced by random disturbance. An average value calculated by using the normalized single-pixel light intensities is applied as a constant threshold shown in Fig. 3(b). With the binarized light intensities obtained by using the constant threshold, CI is applied to recover a correspondence image with conditional

averaging, as shown in Fig. 3(c). No effective object information can be visually rendered, since the usage of one constant threshold ignores dynamic scaling factors induced by random disturbance in the CI system. Therefore, conventional CI performs a blind binarization on the collected light intensities, and would fail under random disturbance. To remove the effect of dynamic and nonlinear scaling factors induced by random disturbance, varying thresholds are estimated by using the proposed WATV algorithm, as shown in Fig. 3(b). Using the series of estimated varying thresholds to binarize light intensities, a correspondence image can be retrieved based on conditional averaging, as shown in Fig.

3(d). Compared to the correspondence image in Fig. 3(c), effective object information has been retrieved, verifying that the estimated varying thresholds are accurate and can facilitate a removal of the effect of the series of dynamic scaling factors induced by random disturbance. It can be seen that the correspondence image in Fig. 3(d) is still of low quality with noise-like background. When the developed CI-PnP is applied with the series of varying thresholds, a reconstructed object image is shown in Fig. 3(e). It can be seen in Fig. 3(e) that the elements are well resolved, and the proposed method facilitates the realization of high-resolution and high-robustness CI against random disturbance.

C. Robustness of the Proposed Method

To further verify robustness of the proposed CI against random disturbance in complex environments, another three objects, i.e., object 1 "bolt", object 2 "paw" and object 3 "plane", are tested by using the experimental setup in Fig. 2(a). These objects are fabricated by leveraging 3D-printing with the feature sizes of 1.0 cm × 1.5 cm, 1.5 cm × 1.5 cm and 1.5 cm × 1.5 cm, respectively. The objects are separately tested, and each object is sequentially illuminated by a series of random patterns with optical waves propagating through complex media, as shown in Fig. 2(a). Here, random disturbance is generated simultaneously from multiple sources using different settings to study the robustness of the proposed CI system. Experimental results are shown in Fig. 4.

In Fig. 4(a), LED currents of the projector are controlled in a range of 200 mA-300 mA to create random disturbance in light source. The light responses of the detector oscillate by alternately using two gains of 20 dB and 30 dB with the switching frequencies randomly selected in a range of 0.2 min ¹ to 0.4 min⁻¹. Single-pixel light intensities collected under random disturbance are normalized by subtracting an average value of the collected light intensities and divided by standard deviation, as shown in Fig. 4(a). A constant threshold is obtained by calculating an average value of the normalized light intensities, as shown in Fig. 4(d). By binarizing the normalized light intensities with the constant threshold, conventional CI cannot retrieve effective object information, as shown in Fig. 4(g). On the contrary, a series of varying thresholds are estimated by using the proposed WATV algorithm, and are applied for the binarization of light intensities. Then, the binarized light intensities are used to recover a correspondence image using conditional averaging, and a reconstructed object image is shown in Fig. 4(i). It is experimentally illustrated that the varying thresholds estimated by using the proposed WATV algorithm are accurate and effective. When the proposed CI-PnP is used with the estimated varying thresholds, a high-quality reconstructed object image can be obtained, as shown in Fig. 4(m).

To increase the disturbance level, LED currents are controlled to fluctuate in a larger range of 100 mA-300 mA in Fig. 4(b). Two gains (i.e., 20 dB and 30 dB) are switched with the higher switching frequencies arbitrarily chosen in a range of 1.0 min⁻¹ to 1.5 min⁻¹. Figure 4(b) shows the normalized

single-pixel light intensities obtained by subtracting an average value of the collected light intensities and divided by standard deviation. Then, a constant threshold is obtained by calculating an average value of the normalized light intensities, as shown in Fig. 4(e). In the proposed method, the varying thresholds estimated by using the WATV algorithm are shown in Fig. 4(e). The recovered correspondence images are shown in Figs. 4(h) and 4(k), when the light intensities are binarized by using the constant threshold and the estimated varying thresholds, respectively. It is demonstrated that the estimated varying thresholds are accurate and effective. When the proposed CI-PnP with the estimated varying thresholds is applied, high-quality object reconstruction can be realized, as shown in Fig. 4(n).

The LED currents are controlled in a larger range of 100 mA-600 mA, and three gains of the detector (i.e., 10 dB, 20 dB and 30 dB) are switched with the higher switching frequencies arbitrarily selected in a range of 1.5 min⁻¹ to 2.0 min-1. After CI under random disturbance is conducted, the normalized light intensities are obtained and shown in Fig. 4(c). More abrupt changes can be observed in the normalized single-pixel light intensities, and this type of random disturbance is applied to illustrate the feasibility of the proposed method in an extremely complex environment. An average value of the normalized light intensities is calculated as a constant threshold, as shown in Fig. 4(f). A series of varying thresholds are also estimated by using the proposed WATV algorithm, as shown in Fig. 4(f). Figure 4(l) shows effective object information rendered in the recovered correspondence image using the estimated varying thresholds, while no object information can be retrieved with a constant threshold as shown in Fig. 4(i). The proposed CI-PnP algorithm with a series of estimated varying thresholds is also applied to realize high-quality object reconstruction, as shown in Fig. 4(o). The developed CI system is experimentally verified to be highly robust against random disturbances with varying disturbance levels using different experimental settings, and high-fidelity object reconstruction can always be implemented.

Different sampling ratios are further tested to verify the proposed method. The reconstructed correspondence images corresponding to object 1 are shown in Figs. 5(a)–5(e), when sampling ratios of 1.0, 0.8, 0.6, 0.4 and 0.2 are used, respectively. It can be seen in Figs. 5(a)–5(e) that the reconstructed objects are of high quality with sharp outlines and clear details. When the sampling ratio is low as 0.2, features of the object are still preserved and visually rendered in Fig. 5(e). The reconstructed correspondence images corresponding to object 2 and object 3 are shown in Figs. 5(f)–5(j) and 5(k)–5(o). It is demonstrated that the proposed method possesses ultra-high robustness against random disturbance under different sampling ratios, and has superior performance at low sampling ratios.

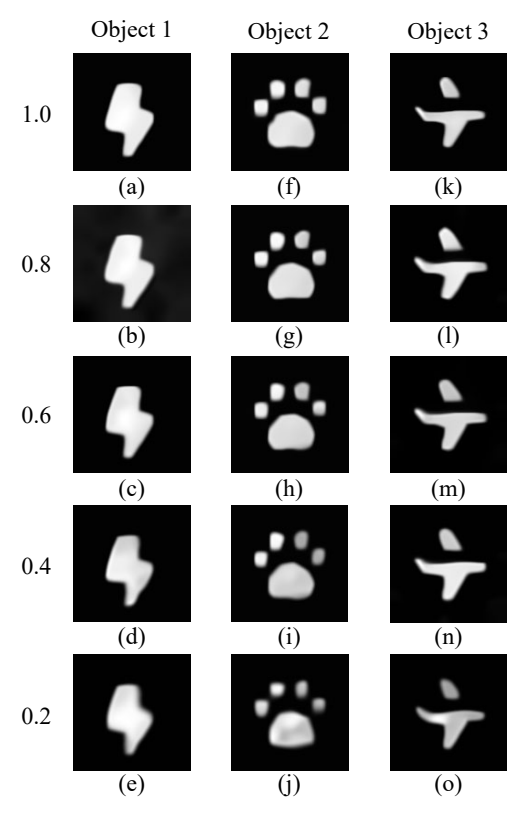


Fig. 5. The recovered correspondence images obtained by using the proposed CI-PnP with estimated varying thresholds under different sampling ratios of 1.0, 0.8, 0.6, 0.4 and 0.2 corresponding to (a)-(e) object 1, (f)-(j) object 2, and (k)-(o) object 3.

D. Comparisons among Different Methods

To show superior performance of the proposed method, different methods are compared under random disturbance, i.e., the proposed CI-PnP with estimated varying thresholds, the method in Ref. [48], CI with a constant threshold, GI [55], differential GI (DGI) [56] and normalized GI (NGI) [57]. Experimental results obtained by using the aforementioned methods are shown in Fig. 6.

Figures 6(a)-6(c) show the reconstructed object images using the proposed method (i.e., the CI-PnP with estimated varying thresholds), and object features are clearly rendered. In Figs. 6(d)–6(f), the reconstructed object images obtained by using the method in Ref. [48] are of low quality due to inaccurate varying-threshold estimations. Conventional CI with a constant threshold fails as shown in Figs. 6(g)-6(i), since the usage of a constant threshold cannot lead to a removal of dynamic scaling factors induced by random disturbance. The usage of one constant threshold introduces a blind binarization on the collected single-pixel light intensities and an incorrect conditional averaging among random patterns. When the collected single-pixel light intensities are applied as correlation coefficients in GI, no object information can be retrieved as shown in Figs. 6(j)-6(l). Although it has been reported that DGI and NGI can be employed for object reconstruction, an inherent problem related to dynamic and nonlinear scaling factors induced by random disturbance is not

solved. DGI and NGI also cannot work as shown in Figs. 6(m)–6(o) and 6(p)–6(r). It is demonstrated that the proposed method is effective and highly robust against random disturbance, and high-quality object reconstruction can be realized in CI under random disturbance.

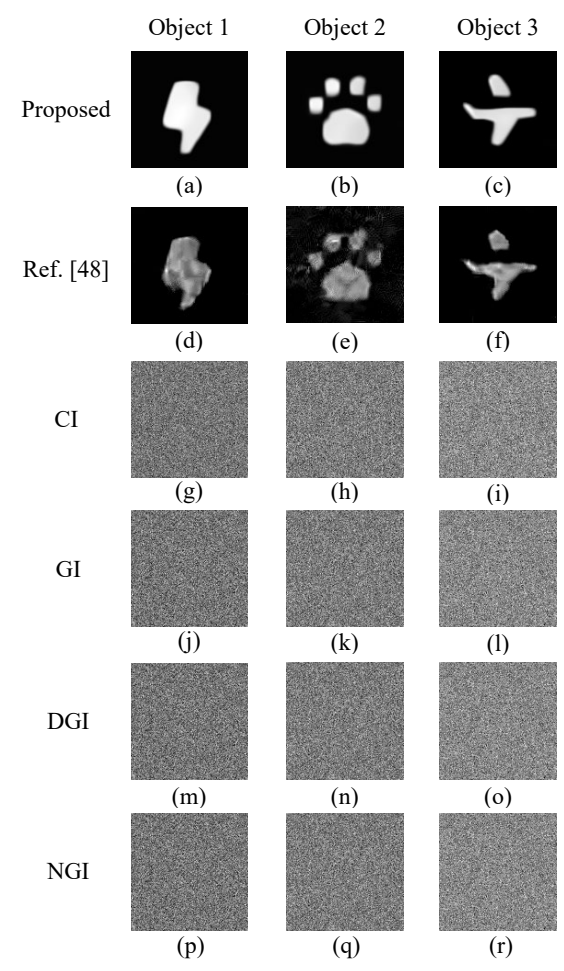


Fig. 6. The reconstructed object images corresponding to object 1, object 2, and object 3 obtained by using (a)-(c) the proposed CI-PnP with the estimated varying thresholds, (d)-(f) the method in Ref. [48], (g)-(i) CI with a constant threshold, (j)-(l) GI, (m)-(o) DGI, and (p)-(r) NGI.

E. The CNR versus Sampling Ratios

To quantitatively evaluate the proposed method, contrast-tonoise ratio (CNR) of the reconstructed object images is employed and calculated by [58]–[62]

$$CNR = \frac{\mu_f - \mu_b}{(\sigma_f + \sigma_b)/2},$$
 (20)

where μ_f and μ_b respectively denote average intensities of feature part (i.e., area of interest) and background part in a reconstructed object image, and σ_f and σ_b denote standard deviation of feature part and background part, respectively.

Figures 7(a)–7(c) show the relationships between the sampling ratios and CNR values of the reconstructed object

images, when CI with a constant threshold, CI with varying thresholds and CI-PnP with varying thresholds are respectively used. As can be seen in Figs. 7(a)–7(c), CNR values of the reconstructed object images obtained by using the CI-PnP with varying thresholds can increase with the higher sampling ratios, and CNR values reach up to 38.16, 33.93 and 38.50, respectively. CNR values of the reconstructed object images obtained by using the proposed CI-PnP with varying thresholds are much larger than those obtained by using other methods. It is quantitatively illustrated in Figs. 7(a)–7(c) that the estimation of a series of varying thresholds is accurate, and the proposed method has superior performance.

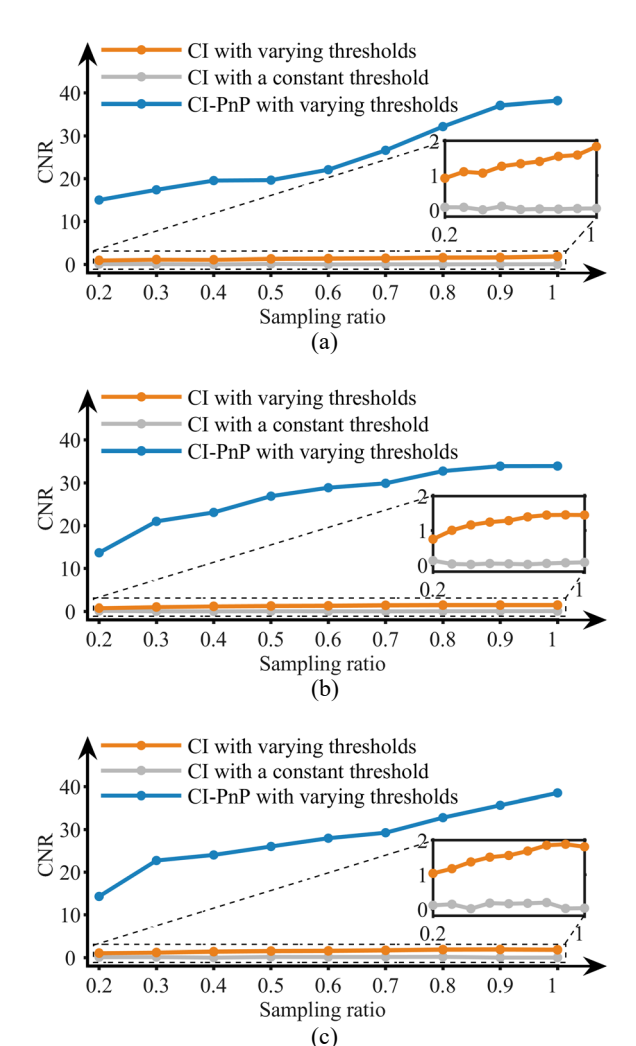


Fig. 7. The relationships between the sampling ratios and CNR values of the reconstructed object images respectively using CI with varying thresholds, CI with a constant threshold and CI-PnP with varying thresholds: (a) object 1, (b) object 2, and (c) object 3.

IV. CONCLUSION

In this paper, we have proposed a robust CI against random disturbances. A series of varying thresholds are accurately estimated by using the WATV algorithm, and are applied to binarize a series of single-pixel light intensities. The binarized light intensities and a series of random patterns are fed into the proposed CI-PnP for object reconstruction. The detailed theoretical descriptions have been given to reveal the fundamentals and formation mechanism. It is demonstrated in optical experiments that the proposed method can effectively remove the effect of dynamic and nonlinear scaling factors induced by random disturbances simultaneously from multiple sources without the usage of temporal carriers, and the reconstructed objects are of high quality. The proposed method opens up an avenue for CI to achieve ultra-high robustness against random disturbances in complex environments, and could be promising in various applications.

REFERENCES

- A. Gnanasambandam and S. H. Chan, "Exposure-referred signal-tonoise ratio for digital image sensors," *IEEE Trans. Comput. Imag.*, vol. 8, pp. 561–575, 2022.
- [2] W. Guicquero, A. Dupret, and P. Vandergheynst, "An algorithm architecture co-design for CMOS compressive high dynamic range imaging," *IEEE Trans. Comput. Imag.*, vol. 2, no. 3, pp. 190–203, 2016.
- [3] M. Jia, Z. Wei, L. Yu, Z. Yuan, and F. Gao, "Noise-disentangled single-pixel imaging under photon-limited conditions," *IEEE Trans. Comput. Imag.*, vol. 9, pp. 594–606, 2023.
- [4] L. Vizioli, S. Moeller, L. Dowdle, M. Akçakaya, F. De Martino, E. Yacoub, and K. Uğurbil, "Lowering the thermal noise barrier in functional brain mapping with magnetic resonance imaging," *Nat. Commun.*, vol. 12, no. 1, pp. 5181–5181, 2021.
- [5] B. Pan, D. Wu, and Y. Xia, "An active imaging digital image correlation method for deformation measurement insensitive to ambient light," *Opt. Laser Technol.*, vol. 44, no. 1, pp. 204–209, 2012.
- [6] D. Shin, A. Kirmani, V. K. Goyal, and J. H. Shapiro, "Photon-efficient computational 3-D and reflectivity imaging with single-photon detectors," *IEEE Trans. Comput. Imag.*, vol. 1, no. 2, pp. 112–125, 2015.
- [7] W. Li, T. Xi, S. He, L. Liu, J. Liu, F. Liu, B. Wang, S. Wei, W. Liang, Z. Fan, Y. Sun, Y. Wang, and X. Shao, "Single-shot imaging through scattering media under strong ambient light interference," *Opt. Lett.*, vol. 46, no. 18, pp. 4538–4541, 2021.
- [8] B. Zhu, J. C. Rasmussen, and E. M. Sevick-Muraca, "Non-invasive fluorescence imaging under ambient light conditions using a modulated ICCD and laser diode," *Biomed. Opt. Express*, vol. 5, no. 2, pp. 562– 572, 2014.
- [9] Y. Mao, C. Flueraru, S. Chang, D. P. Popescu, and M. G. Sowa, "High-quality tissue imaging using a catheter-based swept-source optical coherence tomography systems with an integrated semiconductor optical amplifier," *IEEE Trans. Instrum. Meas.*, vol. 60, no. 10, pp. 3376–3383, 2011.
- [10] M. Ma, L. Gu, Y. Shen, Q. Guan, C. Wang, H. Deng, X. Zhong, M. Xia, and D. Shi, "Computational framework for turbid water single-pixel imaging by polynomial regression and feature enhancement," *IEEE Trans. Instrum. Meas.*, vol. 72, pp. 1–11, 2023.
- [11] S. Zhou, Z. Zhang, Y. Liu, and J. Tian, "Restoration on high turbidity water images under near-field illumination using a light-field camera," *IEEE Trans. Comput. Imag.*, vol. 10, pp. 984–999, 2024.
- [12] S. Mukherjee, A. Vijayakumar, and J. Rosen, "Spatial light modulator aided noninvasive imaging through scattering layers," *Sci. Rep.*, vol. 9, no. 1, pp. 17670–11, 2019.
- [13] N. Chimitt, X. Zhang, Z. Mao, and S. H. Chan, "Real-time dense field phase-to-space simulation of imaging through atmospheric turbulence," *IEEE Trans. Comput. Imag.*, vol. 8, pp. 1159–1169, 2022.
- [14] J. Li and Z. Liu, "Self-measurements of point-spread function for remote sensing optical imaging instruments," *IEEE Trans. Instrum. Meas.*, vol. 69, no. 6, pp. 3679–3686, 2020.
- [15] M. Li, R. Li, S. Bao, Z. Xu, Q. Li, H. Feng, Y. Chen, and H. Chen, "Imaging chain modeling and a scaling experiment for optical remote sensing of lunar surface," *IEEE Trans. Instrum. Meas.*, vol. 73, pp. 1–13, 2024.
- [16] J. Fan, X. Wang, C. Zhou, Y. Ou, F. Jing, and Z. Hou, "Development, calibration, and image processing of underwater structured light vision system: A survey," *IEEE Trans. Instrum. Meas.*, vol. 72, pp. 1–18, 2023.

- [17] Y. Ding, Z. Chen, Y. Ji, J. Yu, and J. Ye, "Light field-based underwater 3D reconstruction via angular re-sampling," *IEEE Trans. Comput. Imag.*, vol. 9, pp. 881–893, 2023.
- [18] M. Jian, X. Liu, H. Luo, X. Lu, H. Yu, and J. Dong, "Underwater image processing and analysis: A review," *Signal Processing. Image Commun.*, vol. 91, p. 116088, 2021.
- [19] I. De Falco, G. Tortora, P. Dario, and A. Menciassi, "An integrated system for wireless capsule endoscopy in a liquid-distended stomach," *IEEE Trans. Biomed. Eng.*, vol. 61, no. 3, pp. 794–804, 2014.
- [20] Q. Cao, R. Deng, Y. Pan, R. Liu, Y. Chen, G. Gong, J. Zou, H. Yang, and D. Han, "Robotic wireless capsule endoscopy: recent advances and upcoming technologies," *Nat. Commun.*, vol. 15, no. 1, pp. 4597–21, 2024
- [21] H. R. Shi, Q. Wang, Y. Zhao, and H. G. Zhang, "High-performance fourier iteration ghost imaging under low sampling rate," *IEEE Trans. Instrum. Meas.*, vol. 73, pp. 1–9, 2024.
- [22] Z. Yang, G. Li, R. Yan, Y. Sun, L. A. Wu, and A. X. Zhang, "3-D computational ghost imaging with extended depth of field for measurement," *IEEE Trans. Instrum. Meas.*, vol. 68, no. 12, pp. 4906–4912, 2019.
- [23] Y. He, Y. Zhou, J. Yu, H. Chen, H. Zheng, J. Liu, Y. Zhou, and Z. Xu, "ADMMNet-based deep unrolling method for ghost imaging," *IEEE Trans. Comput. Imag.*, vol. 10, pp. 233–245, 2024.
- [24] L. Olivieri, J. S. Totero Gongora, L. Peters, V. Cecconi, A. Cutrona, J. Tunesi, R. Tucker, A. Pasquazi, and M. Peccianti, "Hyperspectral terahertz microscopy via nonlinear ghost imaging," *Optica*, vol. 7, no. 2, pp. 186–191, 2020.
- [25] J. Xiong, P. Zheng, Z. Gao, and H. C. Liu, "Algorithm-dependent computational ghost encryption and imaging," *Phys. Rev. Appl.*, vol. 18, no. 3, p. 034023, 2022.
- [26] Z. D. Liu, Z. G. Li, Y. N. Zhao, S. H. Zhang, Z. Y. Ye, D. J. Zhang, H. C. Liu, J. Xiong, and H. G. Li, "Fourier single-pixel imaging via arbitrary illumination patterns," *Phys. Rev. Appl.*, vol. 19, no. 4, p. 044025, 2023.
- [27] Z. Ye, J. Xiong, and H. C. Liu, "Ghost difference imaging using one single-pixel detector," *Phys. Rev. Appl.*, vol. 15, no. 3, p. 034035, 2021.
- [28] D. Liu, M. Tian, S. Liu, X. Dong, J. Guo, Q. He, H. Xu, and Z. Li, "Ghost imaging with non-Gaussian quantum light," *Phys. Rev. Appl.*, vol. 16, no. 6, p. 064037, 2021.
- [29] Y. Yu, J. Zheng, S. Chen, and Z. Yang, "Moving target imaging via computational ghost imaging combined with artificial bee colony optimization," *Trans. Instrum. Meas.*, vol. 71, pp. 1–7, 2022.
- [30] F. Rousset, N. Ducros, A. Farina, G. Valentini, C. D'Andrea, and F. Peyrin, "Adaptive basis scan by wavelet prediction for single-pixel imaging," *IEEE Trans. Comput. Imag.*, vol. 3, no. 1, pp. 36–46, 2017.
- [31] C. Pitsch, D. Walter, L. Gasparini, H. Bürsing, and M. Eichhorn, "3D quantum ghost imaging," Appl. Opt., vol. 62, no. 23, pp. 6275–6281, 2023.
- [32] P. Hong and Y. Liang, "Three-dimensional microscopic single-pixel imaging with chaotic light," *Phys. Rev. A*, vol. 105, no. 2, p. 023506, 2022
- [33] W. Zhao, H. Chen, Y. Yuan, H. Zheng, J. Liu, Z. Xu, and Y. Zhou, "Ultrahigh-speed color imaging with single-pixel detectors at low light level," *Phys. Rev. Appl.*, vol. 12, no. 3, p. 034049, 2019.
- [34] H. Wu, B. Hu, L. Chen, F. Peng, Z. Wang, G. Genty, and H. Liang, "Mid-infrared computational temporal ghost imaging," *Light: Sci. Appl.*, vol. 13, no. 1, p. 124, 2024.
- [35] R. S. Aspden, N. R. Gemmell, P. A. Morris, D. S. Tasca, L. Mertens, M. G. Tanner, R. A. Kirkwood, A. Ruggeri, A. Tosi, R. W. Boyd, G. S. Buller, R. H. Hadfield, and M. J. Padgett, "Photon-sparse microscopy: Visible light imaging using infrared illumination," *Optica*, vol. 2, no. 12, pp. 1049–1052, 2015.
- [36] L. Olivieri, J. S. Totero Gongora, L. Peters, V. Cecconi, A. Cutrona, J. Tunesi, R. Tucker, A. Pasquazi, and M. Peccianti, "Hyperspectral terahertz microscopy via nonlinear ghost imaging," *Optica*, vol. 7, no. 2, pp. 186–191, 2020.
- [37] J. S. Totero Gongora, L. Olivieri, L. Peters, J. Tunesi, V. Cecconi, A. Cutrona, R. Tucker, V. Kumar, A. Pasquazi, and M. Peccianti, "Route to intelligent imaging reconstruction via terahertz nonlinear ghost imaging," *Micromachines*, vol. 11, no. 5, p. 521, 2020.
- [38] D. Pelliccia, A. Rack, M. Scheel, V. Cantelli, and D. M. Paganin, "Experimental X-ray ghost imaging," *Phys. Rev. Lett.*, vol. 117, no. 11, p. 113902, 2016.
- [39] A. Schori and S. Shwartz, "X-ray ghost imaging with a laboratory source," Opt. Express, vol. 25, no. 13, pp. 14822–14828, 2017.

- [40] K. H. Luo, B. Q. Huang, W. M. Zheng, and L. A. Wu, "Nonlocal imaging by conditional averaging of random reference measurements," *Chin. Phys. Lett.*, vol. 29, no. 7, p. 074216, 2012.
- [41] H. Liu, H. Yang, J. Xiong, and S. Zhang, "Positive and negative ghost imaging," Phys. Rev. Appl., vol. 12, no. 3, p. 034019, 2019.
- [42] L. Dou, L. Ren, D. Cao, and X. Song, "Positive-negative ghost imaging with statistics of realizations," *Phys. Rev. Appl.*, vol. 16, no. 4, p. 044013, 2021.
- [43] X. Yao, X. Liu, W. Yu, and G. Zhai, "Ghost imaging based on Pearson correlation coefficients," *Chinese physics B*, vol. 24, no. 5, pp. 340–345, 2015.
- [44] M. Li, Y. Zhang, X. Liu, X. Yao, K. Luo, H. Fan, and L. A. Wu, "A double-threshold technique for fast time-correspondence imaging," *Appl. Phys. Lett.*, vol. 103, no. 21, p. 211119, 2013.
- [45] M. F. Li, Y. R. Zhang, K. H. Luo, L. A. Wu, H. Fan, "Time-correspondence differential ghost imaging," *Phys. Rev. A*, vol 87, no. 3, p. 033813, 2013.
- [46] S. C. Song, M. J. Sun, L. A. Wu, "Improving the signal-to-noise ratio of thermal ghost imaging based on positive–negative intensity correlation," *Opt. Commun.*, vol. 366, pp. 8–12, 2016.
- [47] Y. Xiao, L. Zhou, and W. Chen, "Correspondence imaging through complex scattering media with temporal correction," *Opt. Lasers Eng.*, vol. 174, p. 107957, 2024.
- [48] Z. Xu, Q. Song, and W. Chen, "High-fidelity correspondence imaging in complex media with varying thresholds and 1-bit compressive sensing," *Appl. Phys. Lett.*, vol. 124, no. 11, p. 111105, 2024.
- [49] J. Leng, W. Yu, and S. Wang, "Formation mechanism of correspondence imaging with thermal light," *Phys. Rev. A*, vol. 101, no. 3, p. 033835, 2020.
- [50] H. Yang, S. Wu, H. B. Wang, D. Z. Cao, S. H. Zhang, J. Xiong, K. G. Wang, "Probability theory in conditional-averaging ghost imaging with thermal light," *Phys. Rev. A*, vol. 98, no. 5, p. 053853, 2018.
- [51] L. Bian, J. Suo, Q. Dai, and F. Chen, "Experimental comparison of single-pixel imaging algorithms," J. Opt. Soc. Am. A, vol. 35, no. 1, pp. 78–87, 2018.
- [52] D. Yin and I. W. Selesnick, "Artifact-free wavelet denoising: Nonconvex sparse regularization, convex optimization," *IEEE Signal Process. Lett.*, vol. 22, no. 9, pp. 1364–1368, 2015.
- [53] U. S. Kamilov, H. Mansour, and B. Wohlberg, "A plug-and-play priors approach for solving nonlinear imaging inverse problems," *IEEE Signal Process. Lett.*, vol. 24, no. 12, pp. 1872–1876, 2017.
- [54] K. Dabov, A. Foi, V. Katkovnik, and K. Egiazarian, "Image denoising by sparse 3-D transform-domain collaborative filtering," *IEEE Trans. Image Process.*, vol. 16, no. 8, pp. 2080–2095, 2007.
- [55] J. H. Shapiro, "Computational ghost imaging," *Phys. Rev. A*, vol. 78, no. 6, p. 061802, 2008.
- [56] F. Ferri, D. Magatti, L. A. Lugiato, and A. Gatti, "Differential ghost imaging," Phys. Rev. Lett., vol. 104, no. 25, p. 253603, 2010.
- [57] B. Sun, S. S. Welsh, M. P. Edgar, J. H. Shapiro, and M. J. Padgett, "Normalized ghost imaging," *Opt. Express*, vol. 20, no. 15, pp. 16892–16901, 2012.
- [58] B. Redding, M. A. Choma, and H. Cao, "Speckle-free laser imaging using random laser illumination," *Nat. Photonics*, vol. 6, no. 6, pp. 355– 359, 2012.
- [59] Y. Hao and W. Chen, "A dual-modality optical system for single-pixel imaging and transmission through scattering media," *Opt. Lett.*, vol. 49, no. 2, pp. 371–374, 2024.
- [60] Y. Xiao, L. Zhou, and W. Chen, "High-resolution ghost imaging through complex scattering media via a temporal correction," *Opt. Lett.*, vol. 47, no. 15, pp. 3692–3695, 2022.
- [61] Z. Wang, T. Zhang, Y. Xiao, Z. Liu, and W. Chen, "Common-path ghost imaging through complex media with dual polarization," *Opt. Lett.*, vol. 50, no. 4, pp. 1152–1155, 2025.
- [62] Y. Hao and W. Chen, "Single-pixel complex-field imaging through scattering media," Opt. Lett., vol. 50, no. 6, pp. 1949–1952, 2025.